International Journal of Thermofluids 25 (2025) 101005

Contents lists available at ScienceDirect

International Journal of Thermofluids

journal homepage: www.sciencedirect.com/journal/international-journal-of-thermofluids

# Exploring natural convection and heat transfer dynamics of $Al_2O_3$-$H_2O$ nanofluid in a modified tooth-shaped cavity configuration

Bijan Krishna Saha [a], Jahidul Islam Jihan [b], Goutam Barai [a], Nur Jahangir Moon [a], Goutam Saha [c,d,*], Suvash C. Saha [e,*]

[a] Department of Mathematics, University of Barishal, Barishal 8254, Bangladesh
[b] Department of Mechanical Engineering, Hajee Mohammad Danesh Science and Technology University, Dinajpur 5200, Bangladesh
[c] Department of Mathematics, University of Dhaka, Dhaka 1000, Bangladesh
[d] Miyan Research Institute, International University of Business Agriculture and Technology, Uttara, Dhaka 1230, Bangladesh
[e] School of Mechanical and Mechatronic Engineering, University of Technology Sydney, Ultimo NSW 2007, Australia

ARTICLE INFO

*Keywords:*
Natural convection
Modified tooth-shape cavity
Heat transfer
Nanofluid
Entropy generation

ABSTRACT

*Background:* Heat transfer (HT) is crucial in engineering, particularly for thermal management systems, where elements like a heated rectangular wall, an adiabatic circular cylinder, and nanofluids introduce complexity and improvements. Additionally, exploring the impact of magnetic forces on natural convection (NC) is important in various industrial processes.

*Aims:* The purpose of the study is to examine how different factors influence HT and fluid flow within the cavity. This includes examining the roles of the heated rectangular vertical wall (RVW), the adiabatic circular cylinder, and the magnetic force on the NC of $Al_2O_3$–$H_2O$ nanofluid.

*Method and validations:* This study solves the governing equations and corresponding boundary conditions using Galerkin's weighted residual-based finite element methods. Also, comprehensive comparisons and validations against existing results are conducted to ensure the accuracy of the findings.

*Parameters:* The study involves a range of parameter values, including $0 \leq$ nanoparticle volume fraction ($\varphi$) $\leq$ 5 %, $10^4 \leq$ Rayleigh number ($Ra$) $\leq 10^6$, $0 \leq$ Hartmann number ($Ha$) $\leq 60$.

*Results:* The research reveals that insulated wavy top wall and heated RVW significantly shape the flow field and heat transport. The presence of the adiabatic cylinder further enhances this phenomenon. Incorporating $Al_2O_3$-$H_2O$ nanofluid enhances HT performance, especially at larger $\varphi$.

*Conclusion:* The study concludes that the innovative design approach involving the wavy top wall, heated RVW, and adiabatic circular cylinder significantly influences the heat transfer and flow field within the cavity. This design effectively mitigates external heat loss, demonstrating its potential for improved thermal management systems.

## Introduction

### *Concept definition*

Magnetohydrodynamic (MHD) nanofluids heat transfer (HT) through natural convection (NC) in closed enclosures is of particular interest to both researchers and engineers. This interest stems not only from the unique geometries involved but also from the potential applications in science, engineering, and industry. Studying nanofluids provides insights into thermophysical properties and helps improve HT mechanisms. Recently, HT in NC has gained prominence due to its wide range of applications, incorporating electronic cooling solutions, energy storage technologies, nuclear energy systems, and solar power applications [1].

### *Theoretical review*

Saha et al. [1] sought to thoroughly analyze flow and HT characteristics in different cavity configurations, both with and without the presence of fins, barriers, cylinders, and baffles. This comprehensive analysis explored the impact of various forces on heat transport in

* Corresponding authors.
*E-mail addresses:* bksaha@bu.ac.bd (B.K. Saha), jahidulislam.hstu17@gmail.com (J.I. Jihan), gkgoutam20@gmail.com (G. Barai), moonjahangir51@gmail.com (N.J. Moon), gsahamath@du.ac.bd (G. Saha), Suvash.Saha@uts.edu.au (S.C. Saha).

https://doi.org/10.1016/j.ijft.2024.101005

Available online 5 December 2024

**Nomenclature**

| | |
|---|---|
| Be | Bejan number |
| $Be_l$ | Local Bejan number |
| $C_p$ | Specific heat capacity (j/kgK) |
| $d_f$ | Fluid molecular diameter (nm) |
| $d_p$ | Diameter of nanoparticle (nm) |
| $Nu_{avg}$ | Average Nusselt number |
| $E_{avg}$ | Average entropy generation |
| $E_{gen}$ | Entropy generation |
| L | Length (m) |
| $k_b$ | Boltzmann constant (J/K) |
| M | Molecular weight of the base fluid (kg/mole) |
| N | Avogadro number |
| Pr | Prandtl number |
| *RaRayleigh\ number* | |
| *Re* | Reynolds number |
| Nu | Nusseltnumber |
| $T_{fr}$ | Freezing point of the base fluid (K) |
| k | Thermalconductivity(W/mK) |
| L | Length(m) |
| S | Dimensionlessentropygeneration |
| T | Temperature(K) |
| $T_o$ | Bulktemperature ($T_h + T_c$ /2) (K) |
| u, v | Velocity components in x and y directions (m/s) |
| U, V | Dimensionless velocity components |
| x, y | Dimensional Cartesian coordinates (m) |
| X, Y | Dimensionless Cartesian coordinates |
| $E_t$ | Total entropy generation |
| $B_0$ | Magnetic field |
| φ | Volume fraction |

*Greek Symbols*

| | |
|---|---|
| α | Thermaldiffusivity($m^2$/s) |
| β | Thermalexpansioncoefficient, ($k^{-1}$) |
| ψ | Irreversibility factor |
| ν | Kinematicviscosity($m^2$/s) |
| Θ | Dimensionlesstemperature |
| μ | Viscosity (Ns/$m^{-2}$) |
| ρ | Density (kg/$m^3$) |
| *g* | Gravitational acceleration ($ms^{-2}$) |

*Subscripts*

| | |
|---|---|
| avg | Average |
| nf | Nanofluids |
| f | Base Fluid |
| h | Hot |
| l | Local |
| t | Total |

cavities, including buoyancy, magnetic, and thermophoresis forces, using different fluids. Saha et al. [2] also reviewed HT and entropy generation (Egen) in different types of cavities containing various hybrid nanofluids. To highlight potential directions for future studies in thermal management within enclosures, Saha et al. [3] examined the complex process of Egen in enclosures and suggested several future research directions. Saboj et al. [4] evaluated the optimal HT and Egen within a curved corner cavity to determine the best arrangement for maximizing HT and energy efficiency in winter environments. In another study, Jihan et al. [5] investigated HT and Egen inside a decagonal cavity, with and without a hot obstacle, aiming to establish an improved cooling system for electronic devices such as microprocessors.

Ikram et al. [6] employed second law analysis to investigate Egen properties of an air-filled hexagonal system with an adiabatic dynamical modulator, revealing a 46.91 % increase in Egen as the Reynolds number (Re) ranged from 500 to 1000. Saha et al. [7] examined MHD in a 2D unsteady flow, highlighting the effect of Kerosene-$TiO_2$ nanofluid on HT inside an octagonal wavy cavity. They found that the HT rate increased due to buoyancy-driven forces, particularly in a rectangular vertical wall at the bottom wall's center, with the rate further improving as the volume fraction of the nanofluid (φ) increased. Saboj et al. [8] investigated the HT properties inside an octagonal cavity with a cold inner cylinder, noting that both HT and Egen were enhanced with higher $\varphi$, particularly with $Al_2O_3$–$H_2O$ nanofluid compared to base fluids like water and air. Saha et al. [9] explored the effects of Rayleigh number (Ra) on thermal performance and Egen in nanofluids within a novel tooth-shaped geometry containing a circular cylinder. Finally, Sheremet et al. [10] conducted a quantitative analysis of Egen within a wavy geometry, demonstrating that higher Ra values improved HT, increased convective flow, and altered recirculation patterns in the cavity. These studies collectively provide significant insights into how various factors such as fluid properties, Re and Ra numbers, and cavity geometry influence thermal performance and energy efficiency, guiding the optimization of heat transfer systems.

*Empirical review*

Acharya's investigation [11] studied laminar flow in an octagonal container with a circular cylinder and fins, finding that increases in $\varphi$ and Ra positively affected Egen, while a stronger magnetic field reduced Egen. The study also highlighted that increasing fin height could reduce total Egen, underscoring the importance of fin design in minimizing Egen. Mobedi et al. [12] explored nanofluid convection in a square cavity, noting that higher Ra and thermal conductivity ratios enhanced HT between the walls, with geometric shape significantly influencing flow patterns and HT efficiency. Hatami [13] examined HT in nanofluids within a cavity with two rectangular sides, showing that increasing fin height boosted HT by increasing the heated surface area. Shafee et al. [14] studied Egen in a semi-annulus enclosure with $Fe_3O_4$ nanofluid, revealing that Egen increased with Darcy number (Da), Ra, and Hartmann number (Ha). Alsabery et al. [15] observed that oscillating flexible fins enhanced HT efficiency, particularly with larger oscillation amplitudes.

Recent studies have also focused on the impact of MHD on conventional HT. Ismael & Jasim et al. [16] explored MHD effects in traditional HT systems, while Sheikholeslami et al. [17] studied the role of sinusoidal exterior boundaries on nanofluid temperature transport, finding that Ha decreased the Nusselt number (Nu), while buoyancy force and nanoparticle volume had the opposite effect. Dogonchi et al. [18] analyzed Egen in a cylindrical geometry, finding that curvature increased Egen, with the highest values near the cylinder and curved walls. Sreedevi and Reddy [19] examined HT in a nanofluid-filled square cavity under MHD and thermal radiation, observing enhanced HT with higher magnetic fields and intensified radiation. Tayebi et al. [20] explored the impact of a hollow cylinder on the Egen and NC flow under MHD conditions, noting that the introduction of a conducting cylinder significantly influenced HT and irreversibilities. Kefayati et al. [21] investigated MHD free convection in a cavity with a sinusoidal temperature profile, revealing that a higher buoyancy ratio reduced HT and altered the unyielded zone. Ghasemi et al. [22] studied the cooling of a heat source in a triangular geometry using CuO—$H_2O$ nanofluid, showing that φ influenced HT and that overall performance was affected

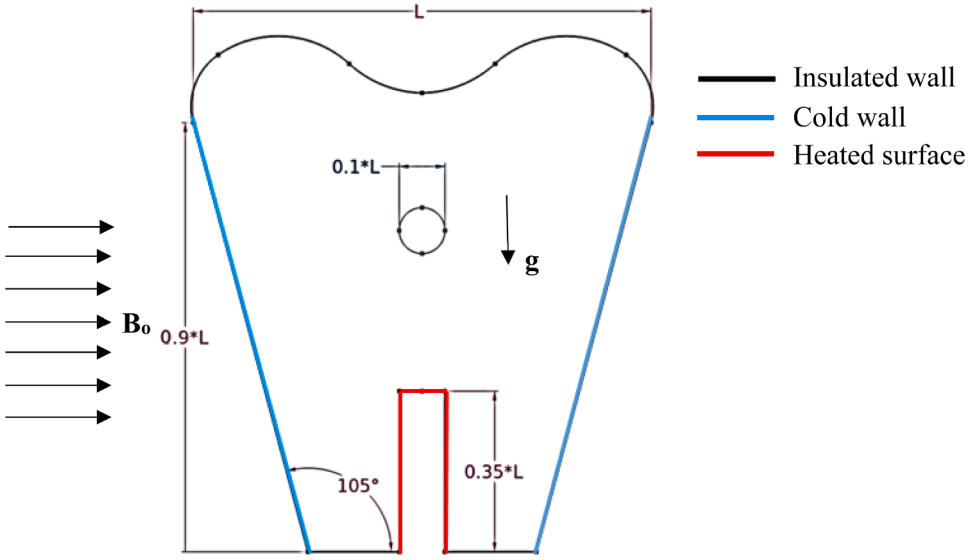


**Fig. 1.** A physical representation of flow domain.

by the inclination angle. Tian et al. [23] analyzed Egen in a square cavity with a square heater, finding that Egen increased with Ra and was minimized at low magnetic fields, while a higher MHD field raised Egen. Finally, Saha et al. [24] investigated the thermal effects of a heated fin in an MHD free convection setup filled with nanofluids, observing a 7.65 % increase in HT with blade-shaped nanoparticles and a 2.86 % increase with spherical nanoparticles. These studies highlight the significant role of nanofluids, fin geometry, MHD effects, and magnetic fields in optimizing HT and minimizing Egen in various thermal systems.

*Novelty of this study*

From our discussion, it's clear that studying HT and Egen in complex domains is crucial. While previous research has explored HT in various cavity structures, including wavy geometries and squares, there has been limited investigation into how modified tooth-shaped cavities affect HT and their potential applications in thermal control systems. Notably, existing studies have not thoroughly examined the influence of unique cavity geometries and boundary conditions, particularly with nanofluids, on HT and overall thermal performance. This study aims to address this gap by analyzing HT dynamics, Egen, and Bejan number (Be) within a cavity featuring a novel modified tooth-shaped geometry. We will investigate how this unique design, in conjunction with nanofluids, impacts HT rates, temperature fields, and thermal performance under specific boundary conditions. The modified tooth-shaped cavities are engineered to optimize space utilization within microprocessors in electronic devices. Their design enhances heat conduction away from the device, helping regulate interior temperature and extend operational time. The rectangular walls of the cavities facilitate efficient heat removal, cooling the device and maintaining a steady temperature throughout the system. This improved thermal management, achieved through enhanced flow circulation, ensures consistent cooling, minimizes internal heat transmission, and ultimately supports better performance and longevity of electronic devices.

## Physical model

In Fig. 1, the physical model represents a modified tooth-shaped cavity with wavy top walls. The $Al_2O_3 - H_2O$ nanofluid within this cavity undergoes steady, 2D, laminar NC in an incompressible liquid medium. An adiabatic cylinder is positioned within the cavity, where 'L' represents its longitudinal dimension and 'r' its radial measurement. The left and right inclined walls are considered cold, the rectangular vertical wall (RVW) serving as the heated wall, the upper wavy wall, the other walls are considered insulated, and gravitational acceleration acts downward. Thermal slip and thermal equilibrium between the conventional fluid and nanoparticles are crucial, as the density of the nanofluid varies during convection, significantly influencing buoyancy. Fig. 1 details the geometric configuration and coordinate systems, while Table 1 provides a comprehensive breakdown of the thermophysical characteristics of various conventional fluids and nanoparticles.

## Mathematical model

To facilitate our analysis, we employed the continuity equation, the momentum equation for laminar flow, and the energy equation to delineate the isothermal contours. The governing equations in 2D Cartesian coordinates, under the previously mentioned assumptions, are expressed as follows [25]:

$$\begin{cases} \dfrac{\partial u}{\partial x}+\dfrac{\partial v}{\partial y}=0 \\ \rho_{nf}\left(u\dfrac{\partial u}{\partial x}+v\dfrac{\partial u}{\partial y}\right)=-\dfrac{\partial p}{\partial x}+\mu_{nf}\left(\dfrac{\partial^2 u}{\partial x^2}+\dfrac{\partial^2 u}{\partial y^2}\right) \\ \rho\left(u\dfrac{\partial v}{\partial x}+v\dfrac{\partial v}{\partial y}\right)=-\dfrac{\partial p}{\partial y}+\mu\left(\dfrac{\partial^2 v}{\partial x^2}+\dfrac{\partial^2 v}{\partial y^2}\right)+(\rho\beta)_{nf}g(T-T_c)-\sigma_{nf}{B_0}^2 v \\ \left(u\dfrac{\partial T}{\partial x}+v\dfrac{\partial T}{\partial y}\right)=\alpha_{nf}\left(\dfrac{\partial^2 T}{\partial x^2}+\dfrac{\partial^2 T}{\partial y^2}\right) \end{cases} \tag{1a}$$

*Dimensional boundary conditions:*

$$\begin{cases} \text{On the left and right walls :} & u=v=0,\ T=0 \\ \text{On rectangular wall surface :} & u=v=0,\ T=1 \\ \text{Remaining walls :} & u=v=0,\ \dfrac{\partial T}{\partial x}=0 \end{cases} \tag{1b}$$

The following thermal and physical characteristics are listed [26,27]:

**Table 1**
Thermo-physical properties of $H_2O$ and $Al_2O_3$ nanoparticles [5,8].

| Water/ Nanoparticles | $C_p$ $[JKg^{-1}K^{-1}]$ | ρ $[Kgm^{-3}]$ | $k$ $[Wm^{-1}k^{-1}]$ | μ $[Kgm^{-1}s^{-1}]$ | $\beta \times 10^5$ $[K^{-1}]$ | σ $[Sm^{-1}]$ | $Pr$ |
|---|---|---|---|---|---|---|---|
| Water ($H_2O$) | 4179 | 997.1 | 0.613 | 0.001003 | 21 | $5.5 \times 10^{-5}$ | 6.8377 |
| Alumina ($Al_2O_3$) | 765 | 3970 | 40 | – | 0.85 | $3.5 \times 10^{7}$ | – |

$$\begin{cases} \rho_{nf} = (1-\varphi)\rho_f + \varphi\rho_s \\ \mu_{nf} = \mu_f(1-\varphi)^{-2.5} \\ \alpha_{nf} = \dfrac{k_{nf}}{(\rho c_p)_{nf}} \\ \dfrac{k_{nf}}{k_f} = 1 + 4.4Re_p^{0.4}Pr_f^{0.66}\left(\dfrac{T}{T_{fr}}\right)^{10}\left(\dfrac{k_p}{k_f}\right)^{0.03}\varphi^{0.66} \\ \dfrac{\mu_f}{\mu_{nf}} = 1 - 34.87\left(\dfrac{d_p}{d_f}\right)^{-0.3}\varphi^{1.03} \\ (\rho c_p)_{nf} = (1-\varphi)(\rho c_p)_f + \varphi(\rho c_p)_s \\ (\rho\beta)_{nf} = (1-\varphi)(\rho\beta)_f + \varphi(\rho\beta)_s \\ \dfrac{(\rho\beta_T)_{nf}}{(\rho\beta_{T\beta})_f} = (1-\varphi) + \varphi\dfrac{(\rho\beta_T)_p}{(\rho\beta_T)_f} \\ \sigma_{nf} = \dfrac{\sigma_s + 2\sigma_f - 2(\sigma_f - \sigma_s)\varphi}{\sigma_s + 2\sigma_f + (\sigma_f - \sigma_s)\varphi}\sigma_f \end{cases} \tag{2}$$

where,

$$Re_p = \frac{2\rho_f k_b T}{\pi\mu_f^2 d_p},\ d_f = 0.1\left(\frac{6M}{N\pi\rho_f}\right)^{\frac{1}{3}}$$

The following transformations are used to reform the governing equations (1a) [28,29]:

$$X = \frac{x}{L},\ Y = \frac{x}{L},\ U = \frac{uL}{\alpha_f},\ V = \frac{vL}{\alpha_f},\ \theta = \frac{(T_f - T_c)}{(T_h - T_c)},\ P = \frac{pL^2}{\rho_{nf}\alpha_f{}^2},$$

$$D = \frac{d}{L},\ H = \frac{h}{L},\ B = \frac{b}{L},\ R = \frac{r}{L} \tag{3}$$

Non-dimensional governing equation:

$$\begin{cases} \dfrac{\partial U}{\partial X} + \dfrac{\partial V}{\partial Y} = 0 \\ U\dfrac{\partial U}{\partial X} + V\dfrac{\partial U}{\partial Y} = -C_0\dfrac{\partial P}{\partial X} + \mathrm{Pr}C_1\left(\dfrac{\partial^2 U}{\partial X^2} + \dfrac{\partial^2 U}{\partial Y^2}\right) \\ U\dfrac{\partial V}{\partial X} + V\dfrac{\partial V}{\partial Y} = -C_0\dfrac{\partial P}{\partial Y} + C_2\left(\dfrac{\partial^2 V}{\partial X^2} + \dfrac{\partial^2 V}{\partial Y^2}\right) + C_3\theta - C_4 V \\ U\dfrac{\partial \theta}{\partial X} + V\dfrac{\partial \theta}{\partial Y} = C_5\left(\dfrac{\partial^2 \theta}{\partial X^2} + \dfrac{\partial^2 \theta}{\partial Y^2}\right) \end{cases} \tag{4a}$$

Where,

$$C_0 = \frac{\rho_f}{\rho_{nf}},\ C_1 = \frac{\rho_f\mu_{nf}}{\rho_{nf}\mu_f},\ C_2 = \frac{Pr\rho_f\mu_{nf}}{\rho_{nf}\mu_f},\ C_3 = \frac{(\rho\beta)_f RaPr}{\rho_{nf}\beta_f},\ C_4 = \frac{\rho_f\sigma_{nf}\ Ha^2 Pr}{\rho_{nf}\sigma_f},\ C_5 = \frac{\alpha_{nf}}{\alpha_f}$$

Non-dimensionless boundary conditions:

$$\begin{cases} \text{On the left and right walls :} & U = V = 0,\ \theta = 0 \\ \text{On rectangular wall surface :} & U = V = 0,\ \theta = 1 \\ \text{Remaining walls :} & U = V = 0,\ \dfrac{\partial\theta}{\partial X} = 0 \end{cases} \tag{4b}$$

Average Nusselt Number and total Egen [7,30]:

$$\begin{cases} Nu_{avg} = \dfrac{k_{nf}}{k_f}\displaystyle\int_S \frac{\partial\theta}{\partial Y}dX \\ E_t = \psi\dfrac{\mu_{nf}}{\mu_f}\left[2\left(\dfrac{\partial U}{\partial X}\right)^2 + 2\left(\dfrac{\partial V}{\partial Y}\right)^2 + \left(\dfrac{\partial U}{\partial Y} + \dfrac{\partial V}{\partial X}\right)^2\right] + \dfrac{k_{nf}}{k_f}\left[\left(\dfrac{\partial\theta}{\partial X}\right)^2 + \left(\dfrac{\partial\theta}{\partial Y}\right)^2\right] \end{cases} \tag{5}$$

where ψ is $10^{-4}$ and S is the heated surface.

Average Egen, the local and average *Be* are presented as follows [31]:

$$\begin{cases} E_{avg} = \dfrac{\int\int E_t\ \mathrm{dX}\ \mathrm{dY}}{\int\int\ \mathrm{dX}\ \mathrm{dY}} \\ Be_l = \dfrac{k_{nf}}{k_f}\left[\left(\dfrac{\partial\theta}{\partial X}\right)^2 + \left(\dfrac{\partial\theta}{\partial Y}\right)^2\right] \Big/ E_t \\ Be_{avg} = \dfrac{\int_A\int_A Be_l\ \mathrm{dX}\ \mathrm{dY}}{\int_A\int_A\ \mathrm{dX}\ \mathrm{dY}} \end{cases} \tag{6}$$

## Grid independence test, method and validation

Fig. 2 illustrates the modified tooth-shaped cavity with circular obstacles. To ensure the accuracy of the study, a grid independence test

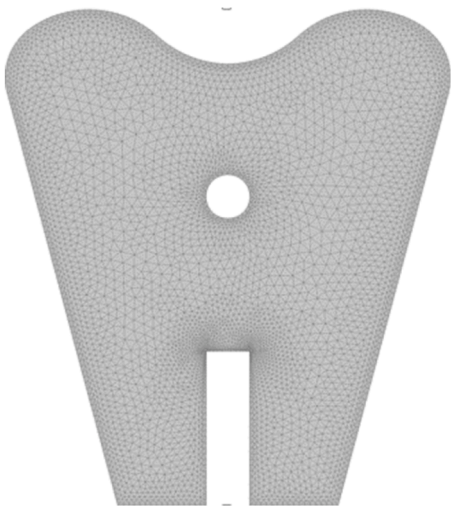

**Fig. 2.** Schematic presentation of the grid Modified Tooth cavity with obstacles.

was performed, as shown in Table 2 in order to offering a balance between result accuracy and computational cost. In this study, a triangular mesh with corner refinement was utilized. We experimented with various element sizes ranging from 21,802 to 48,358. Based on our comparisons, we selected an element size of 44,338, which resulted in an error of <0.0752 %.

In this research, the computational domain is divided into a series of non-overlapping regions called elements. The Galerkin method is then used to convert the nonlinear governing partial differential equation into a system of integral equations that can be solved numerically. And simulations are conducted utilizing COMSOL Multiphysics 6.1. Also, Fig. 3 shows a graphical representation of our research approach.

The isothermal and streamline profiles at Ra values of $10^4$ and $10^5$ in a octagon cavity were analyzed to verify the numerical results presented in Fig. 4. The findings align with the earlier research [8], which focused on octagon domain. To increase confidence in the current computer simulation, comparisons were made with other published papers. Additionally, Fig. 5 presents a comparative analysis between our isothermal contour results and those from an experimental study [32]. It involves a rectangular air-filled enclosure heated by a localized source named rectangular vertical wall (RVW). The chart demonstrates a strong correspondence between the obtained results. Moreover, a quantitative comparison highlights a high degree of accuracy and reliability with the results obtained from the previously analyzed model shown in Table 3.

## Result and discussion

The study investigates the magnetohydrodynamics HT in a NC within a modified tooth shape cavity, coupled with a rectangular wall attached to a horizontal wall and an adiabatic circular cylinder. The investigation is conducted considering $10^4 \leq Ra \leq 10^6$, $0 \leq \varphi \leq 5$ %, circular cylinder *Ra*dius (*r*) of 0.05, and Ha from 0 to 60. The dimensions of RVW include a height of 0.35 and a width of 0.09879. For the analysis of NC, two distinct cases are discussed: Case I: Involving a modified tooth-shaped cavity with varying Ha across different $0 \leq \varphi \leq 5$ % at a fixed Ra of $10^5$. Case II: Encompassing a modified tooth-shaped cavity with various $10^4 \leq Ra \leq 10^6$ across different $0 \leq \varphi \leq 5$ % at a constant Ha of 10.

### *Case I: The effect of the nanoparticle concentration and Rayleigh number*

In Fig. 6, the isotherm contours demonstrate a dependency on two critical factors: $\varphi$ and Ra. In each scenario, these contours exhibit a seamless distribution across the entire cavity. Notably, as Ra increases, the thermal performance within the cavity improves. At $Ra = 10^4$, the isotherm contours form parallel curves extending from the bottom to the top wavy wall, maintaining symmetrical distribution across varying $\varphi$ from 0.03 to 0.05. Upon reaching $Ra = 10^5$, the contours, although still parallel, exhibit a subtle twist closer to the adiabatic surface, yet remain symmetrically distributed from bottom to top. Finally, at $Ra = 10^6$, the contours adopt a twisted configuration from the bottom wall to the two-sided wall, while still maintaining symmetrical distribution across different $\varphi$ values. Fig. 6 also presents streamline contours at various $\varphi$, demonstrating a dependency on Ra. Thermal buoyancy forces appear weaker at lower $Ra = 10^4$. Distinctive streamline contours emerge across different $Ra = 10^4$ to $10^6$, exhibiting smooth rotations and vortices throughout the cavity. Notably, the configuration remains consistent across varying $\varphi$ at the same Ra. As Ra increases, the streamline contours form more spaced curves within the enclosure, displaying two vortices at higher Ra, with counterclockwise rotation on the left and clockwise rotation on the right.

**Table 2**
Grid Independence Test for $Nu_{avg}$ ($Ra = 10^6$).

| No. of the Elements | $Nu_{avg}$ | $\lvert Error \rvert$ |
|---|---|---|
| 21,802 | 13.214 | – |
| 27,750 | 13.293 | 0.5943 % |
| 44,338 | 13.303 | 0.0752 % |
| 48,358 | 13.302 | 0.0075 % |

Fig. 7 presents variation of $S_{lhd}$, $S_{lfd}$, $E_{total,}$ and $Be_l$ for various Ra. It is observed that a rise in Ra enhances buoyancy-driven convection, which can lead to stronger velocity and temperature gradients. These stronger gradients increase viscous and thermal dissipation, resulting in higher overall Egen despite the appearance of the MHD effects. When $S_{lhd}$ is dominant, it leads to an increase in the numbers of the contour along the cold walls and the contour becomes stronger and no vortices can be found near the bottom wall or along with the cylinder. As a result, the contours become more linear HT along the cold walls and cylinder, which in turn helps to reduce the temperature fluctuation within the flow pattern. On the other hand, when fluid friction (FF) becomes dominant inside the domain, then by raising Ra values, additional vortices emerge near the non-conductive cylinder and cold walls, which leads to enhance HT throughout the geometry since viscous dissipation is more significant than HT. Due to this, the contours are closer to the cylinder and the cold walls, leading to a smoother flow pattern near the walls as FF increases. However, in case of Be number, as Ra increases, the number of contours decrease throughout the geometry and goes closer to the cold and heated walls, which exhibits more efficient HT.

### *Quantitative analysis*

*Average nusselt number ($Nu_{avg}$).* Table 4 demonstrates the influence of Ra and $\varphi$ on the system with Ha = 10. As both $\varphi$ and Ra increase, there's a corresponding increase in $Nu_{avg}$. Notably, thermal performance is enhanced for larger $\varphi = 0.05$ particularly when the Ra is elevated. At $Ra = 10^4$, the table shows the lowest $Nu_{avg}$ value but with increasing Ra indicates stronger buoyancy forces, which enhance convective currents within the fluid. These stronger currents improve the rate of HT from the heated surface to the bulk fluid, increasing the Nu. As a result, $Nu_{avg}$ increase for $Ra = 10^4$ to $10^6$ for each $\varphi$.

As both the volume fraction ($\varphi$) and Ra increase, there's a corresponding increase in $Nu_{avg}$ as shown in Table 4. Because of the modified cavity structure, more heat is directed toward the cold wall, and with the heat source at the bottom, heat spreads more evenly across the surface. Moreover, the insertion of nanofluids further increases the buoyancy forces, which enhances this heat distribution and ultimately increases the overall Nu.

*Entropy generation (Egen).* Table 5 demonstrates that with an increase in $Ra = 10^4$ to $10^6$, $\varphi = 0$ to 5 %, Egen escalates slightly, indicating potential areas for enhancing system efficiency. However, an opposite phenomenon can be observed when $\varphi$ is increased, as nanofluids comparatively minimize fluctuations in HT, resulting in less variation in Egen. But at $Ra = 10^6$ and$\varphi = 0.03$, overall, $E_{gen}$ peaks, signifying the complete transition of flow behavior into convection. This transition induces chaos within the geometry as convection becomes dominant and as a result, the overall Egen is increased significantly. As $\varphi$ increases, the overall Egen is slightly reduced due to nanofluid that improved HT capacity.

*Average bejan number ($Be_{avg}$).* The distributions of Be reveal a noteworthy contribution of irreversibility stemming from HT processes in generating total Egen within the cavity. Notably, the predominance of irreversibility attributed to HT in the overall Egen is influenced by the flow dynamics within the system. This influence becomes more pronounced with increasing φ and decreasing Ra, as evidenced by the Be values presented in Table 6. Moreover, as the Ra increases, Be decreases significantly, indicating that HT due to conduction becomes more dominant compared to HT by convection.

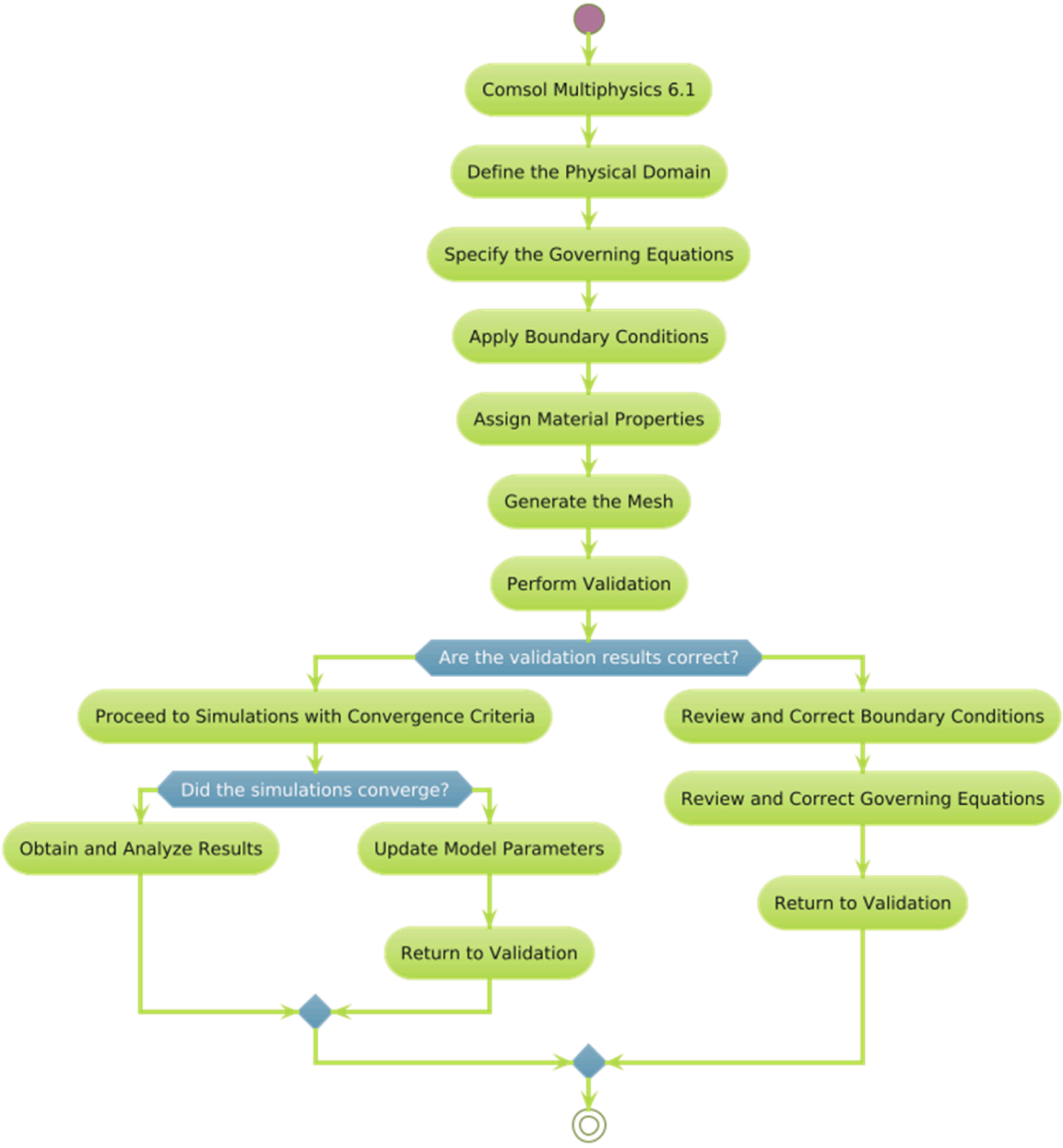


**Fig. 3.** Flowchart of Numerical simulation.

*Case II: The effect of the nanoparticle concentrations and Hartmann number*

In Fig. 8, it is apparent that the isotherm contours are influenced by two primary factors: the nanoparticle volume fractions in the nanofluids and Ha. Across all scenarios, these contours exhibit a smooth distribution throughout the cavity. Notably, as Ha value rises, there is a corresponding decline in thermal performance, even as $\varphi$ within the cavity rise. At Ha = 0, the isotherm contours form parallel curves with subtle twists from the bottom to the top wavy wall, evenly distributed across different $\varphi$ (= 0.03, 0.04, 0.05). With Ha increasing to 20, the contours maintain their parallel orientation, positioning closer to the adiabatic surface from the bottom to the top wavy wall, while still maintaining symmetry in distribution. Likewise, at Ha = 50, the isotherm contours persist as parallel lines from the lower to the upper wall inside the cavity, symmetrically distributed across various φ. Interestingly, thermal performance declines as Ha increase at constant φ, and vice versa.

As can be seen in Fig. 8, two critical factors also impact the streamline contours: Ha and $\varphi$ in the nanofluids. The flow appears symmetrical and fluid across all streamline shapes. Significantly, at various Ha values, negligible distortion is seen in the streamlines as $\varphi$ increase. Two separate vortices occur at lower Ha values; the right vortex rotates clockwise, while the left one rotates counterclockwise direction. Notably, at Ha = 0 and $\varphi$ = 0, the left vortex's flow intensity is more prominent. However, there is a noticeable decrease in flow strength when Ha and $\varphi$ increase.

Additionally, Egen and Be can be influenced by Ra, φ and Ha as illustrated in Fig. 9. Here, with Ra and φ considered fixed, Egen can be influenced by Ha, as the MHD field (quantified by Ha) can affect the overall heat transfer rates. The Lorentz force produced by the MHD field counteracts the motion of the electrically conducting nanofluid, thereby suppressing convective flow. With reduced convective flow, the temperature distribution becomes more uniform, leading to smaller temperature gradients. Since thermal Egen is directly related to temperature gradients, a reduction in these gradients results in lower Egen. Also, the magnetic effect reduces Egen due to viscous dissipation by damping

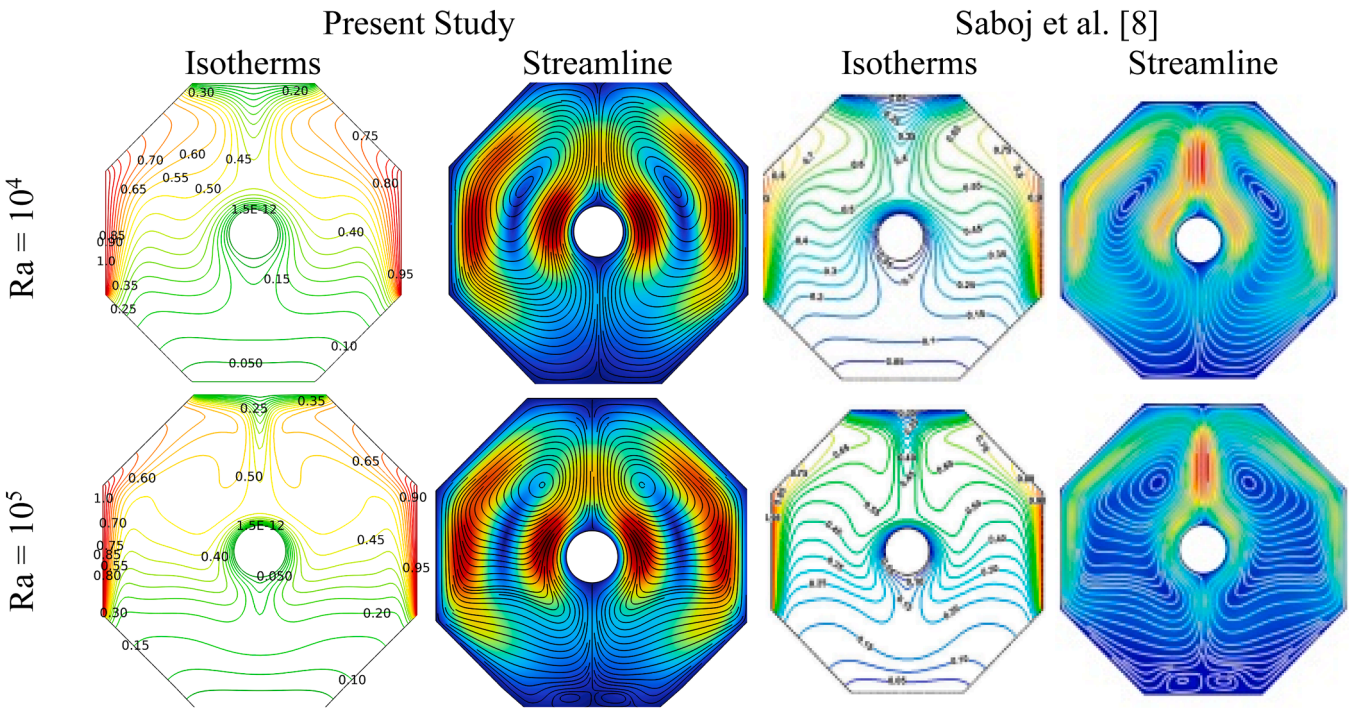


**Fig. 4.** Comparison between present and numerical results [8] results for (i) Ra = $10^4$ and (ii) Ra = $10^5$ at Pr = 6.8377.

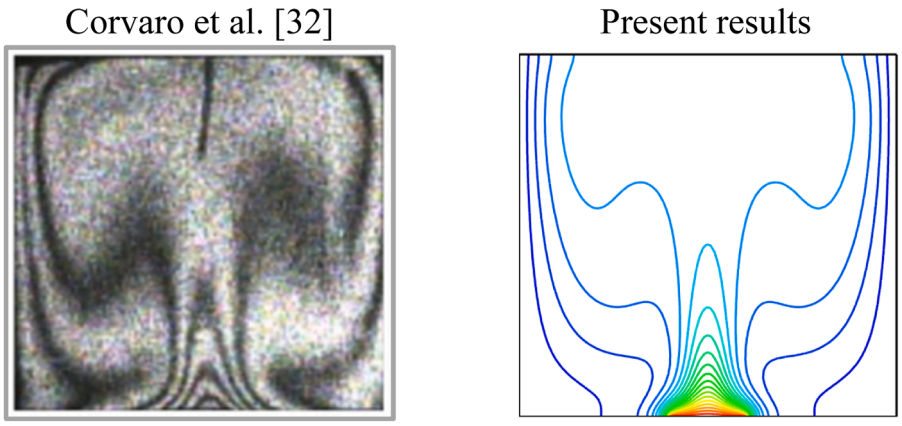


**Fig. 5.** Comparison between present and experimental results [32] for $Ra = 2.02 \times 10^5$.

**Table 3**
Comparison of the present results and numerical results [8] for Pr = 0.71, Ha = 0.

| *Ra* | $Nu_{avg}$ | | Error (%) |
|---|---|---|---|
| | Saboj et al. [8] | Present | |
| $10^4$ | 4.20 | 4.2032 | 0.0761 % |
| $10^5$ | 6.81 | 6.8270 | 0.24963 % |
| $10^6$ | 11.22 | 11.262 | 0.3743 % |

fluid motion, stabilizing the flow, producing a more uniform velocity profile. However, the MHD field can enhance the effective thermal conductivity of the nanofluid, resulting in more uniform temperature distributions and reduced thermal gradients. As a result, the HT irreversibility decreases, contributing to a potential increase in Be.

*Quantitative analysis*

*Average nusselt number ($Nu_{avg}$).* Fig. 10 showcases the influence of Ha and $\varphi$ when Ra = $10^5$. The existence of a magnetic field increases the effective viscosity of the fluid. This increased viscosity further dampens the fluid motion and reduces the convective HT, contributing to a lower Nu. It is evident that as Ha increases, the corresponding $Nu_{avg}$ decreases for each $\varphi$. On the other hand, nanoparticles can enhance the natural convective currents within the fluid, improving overall convective HT. This enhancement is particularly significant at higher $\varphi$, contributing to an increased Nu value. For each Ha, with increasing $\varphi$, the corresponding $Nu_{avg}$ increases due to enhanced convective HT. Remarkably, when $\varphi$ = 0.00 and Ha = 60, the $Nu_{avg}$ is the lowest, but when Ha = 0, the $Nu_{avg}$ is the highest, as illustrated in Fig. 10.

*Entropy generation ($E_{gen}$).* Fig. 11 reveals a notable trend: entropy generation increases with decreasing Ha and $\varphi$. At very low Ha, the magnetic influence on the flow is minimal, allowing convection to dominate, thereby generating more disturbance and consequently higher overall

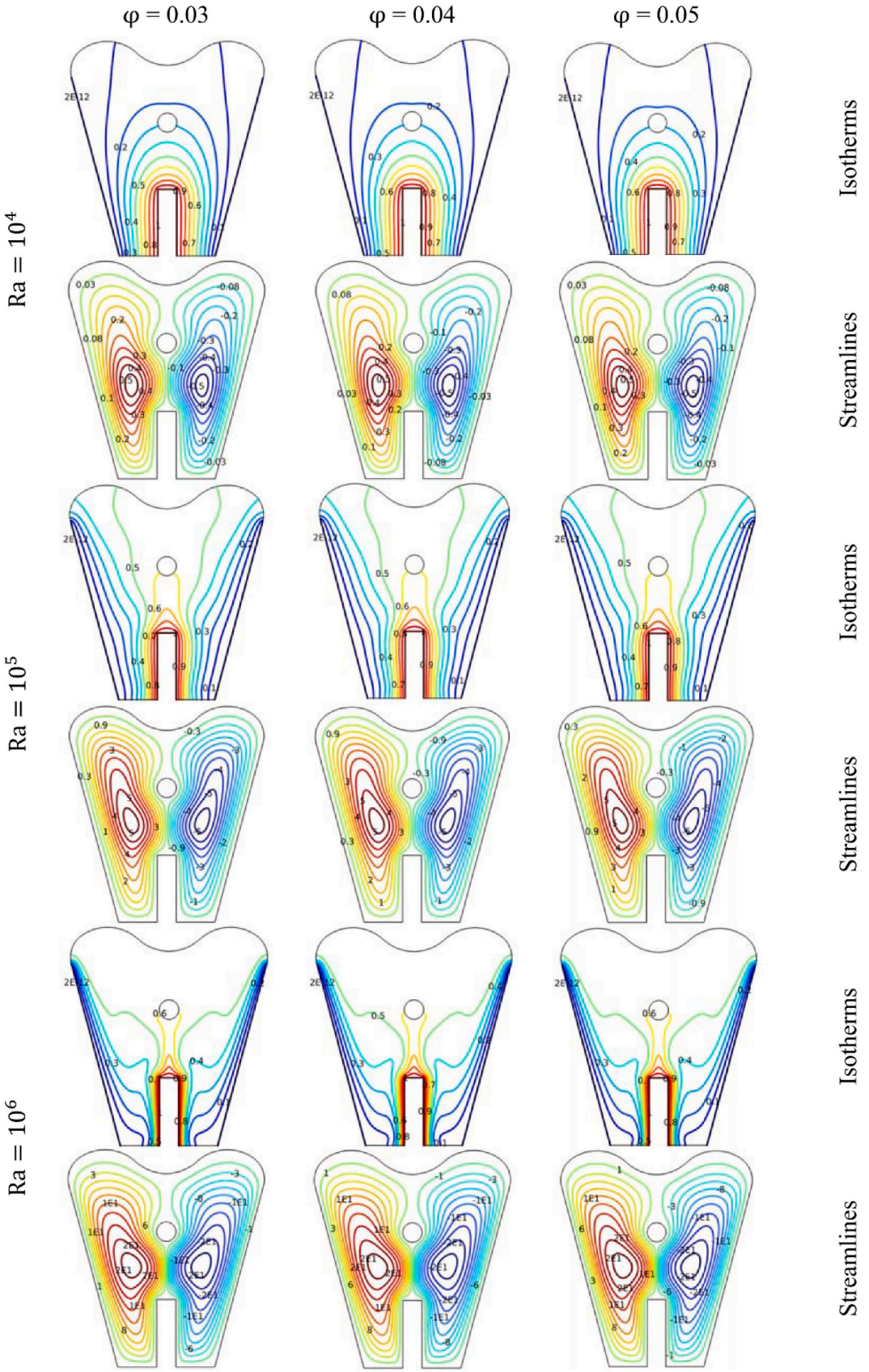


**Fig. 6.** Isotherm and streamline contours for various φ across different Ra, with Ha = 10, Pr = 6.84.

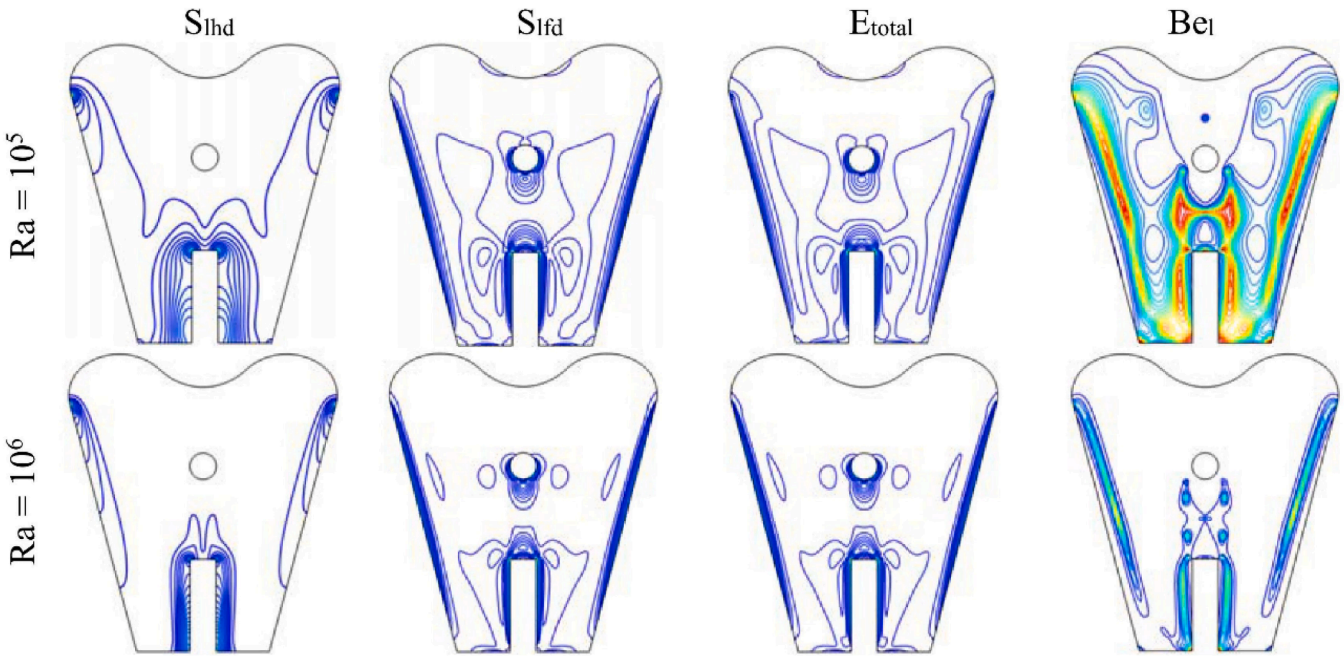


**Fig. 7.** Variation of $S_{lhd}$, $S_{lfd}$, $E_{total,}$ and $Be_l$ with Ra at Ha = 10 and φ = 0.04.

**Table 4**
$Nu_{avg}$ variation with *Ra* and *φ* for *Ha* = 10.

| *φ* | Ra = $10^4$ | Ra = $10^5$ | Ra = $10^6$ |
|---|---|---|---|
| φ = 0.00 | 4.06 | 6.05 | 12.48 |
| φ = 0.01 | 4.23 | 6.20 | 12.83 |
| φ = 0.02 | 4.33 | 6.27 | 13.01 |
| φ = 0.03 | 4.41 | 6.32 | 13.14 |
| φ = 0.04 | 4.48 | 6.37 | 13.26 |
| φ = 0.05 | 4.55 | 6.40 | 13.36 |

Egen. As a result, when *φ* = 0 and Ha = 0, Egen becomes the highest. However, as Ha increases, the magnetic forces become more dominant, altering the flow patterns. This dominance shapes the flow behaviour, reducing disturbances and promoting smoother flow patterns throughout the system. Moreover, increasing *φ* of nanofluids enhances this effect, leading to smoother flow patterns and lower Egen. As shown in Fig. 11, when Ha = 60, Egen shows another trend, with increasing *φ*, Egen slightly increases.

**Table 5**
Entropy generation variation with different *Ra* and *φ* for *Ha* = 10.

| φ | Ra = $10^4$ | Ra = $10^5$ | Ra = $10^6$ |
|---|---|---|---|
| φ = 0.00 | 4.30 | 28.18 | 551.31 |
| φ = 0.01 | 4.47 | 28.25 | 561.94 |
| φ = 0.02 | 4.56 | 28.06 | 564.90 |
| φ = 0.03 | 4.64 | 27.81 | 565.95 |
| φ = 0.04 | 4.71 | 27.52 | 555.86 |
| φ = 0.05 | 4.77 | 27.21 | 564.98 |

**Table 6**
Bejan number variation with different Ra and φ for Ha = 10.

| φ | Ra = $10^4$ | Ra = $10^5$ | Ra = $10^6$ |
|---|---|---|---|
| φ = 0.00 | 0.873 | 0.221 | 0.0298 |
| φ = 0.01 | 0.880 | 0.226 | 0.0302 |
| φ = 0.02 | 0.884 | 0.231 | 0.0306 |
| φ = 0.03 | 0.889 | 0.235 | 0.0309 |
| φ = 0.04 | 0.893 | 0.240 | 0.0312 |
| φ = 0.05 | 0.897 | 0.244 | 0.0315 |

*Average bejan number ($Be_{avg}$).* As *φ* increases, the reduction in thermal irreversibility tends to be more substantial than the increase in viscous dissipation, leading to an increase in Be. In every case of Ha, Be increased with increasing *φ*, which is illustrated in Fig. 12. Here, for every case of *φ*, with increasing Ha, the magnetic field reduces FF irreversibility by damping fluid motion, thereby making HT irreversibility more dominant in the system. This results in a higher ratio of HT irreversibility to the total irreversibility, leading to an increased Be. Remarkably, Be become the highest when Ha = 60 and *φ* = 0.5 and the lowest at Ha = 0, *φ* = 0.

## Conclusion

This research presents a comprehensive numerical analysis into HT phenomena within a closed complex cavity, with a specific focus on the effects of a rectangular vertical wall and an adiabatic circular cylinder. Additionally, the study explores the influence of MHD force on NC, particularly in nanofluids comprising $Al_2O_3$nanoparticles dispersed in water. Present study reveals that nanoparticles enhance interparticle drag forces, promoting rapid stabilization. As volume fraction and Ra increase, $Nu_{avg}$ increase. Thermal performance is enhanced for larger nanoparticle volumes, particularly when Ra is higher. Entropy generation analysis helps evaluate system effectiveness by identifying areas of inefficiency and guiding toward more efficient designs. The incorporation of nanofluids promotes more uniform flow, reduces Egen, and enhances magnetic forces, reducing disturbances and promoting smoother flow patterns. The main findings are summarized below:

- For fixed Ra = $10^6$and Ha = 10, Average Nusselt Numbers are increased 7.05 % varying volume fraction φ = (0.00 − 0.05).
- Average Nusselt Numbers are decreased 29.50 % for varying Ha = (0 to 60) for Ra = $10^5$ and φ = 0.05 while Average Nusselt Numbers increase 10.78 % for varying φ = (0.00 − 0.05) with fixed Ha = 60 and for Ra = $10^5$.
- Entropy generation become height in cases-II when Ha = 0, φ = 0.02 and become lowest when Ha = 60, φ = 0.00 with fixed Ra = $10^5$.
- Entropy generation becomes the highest when Ra = $10^6$, φ = 0.03 with fixed Ha = 10.

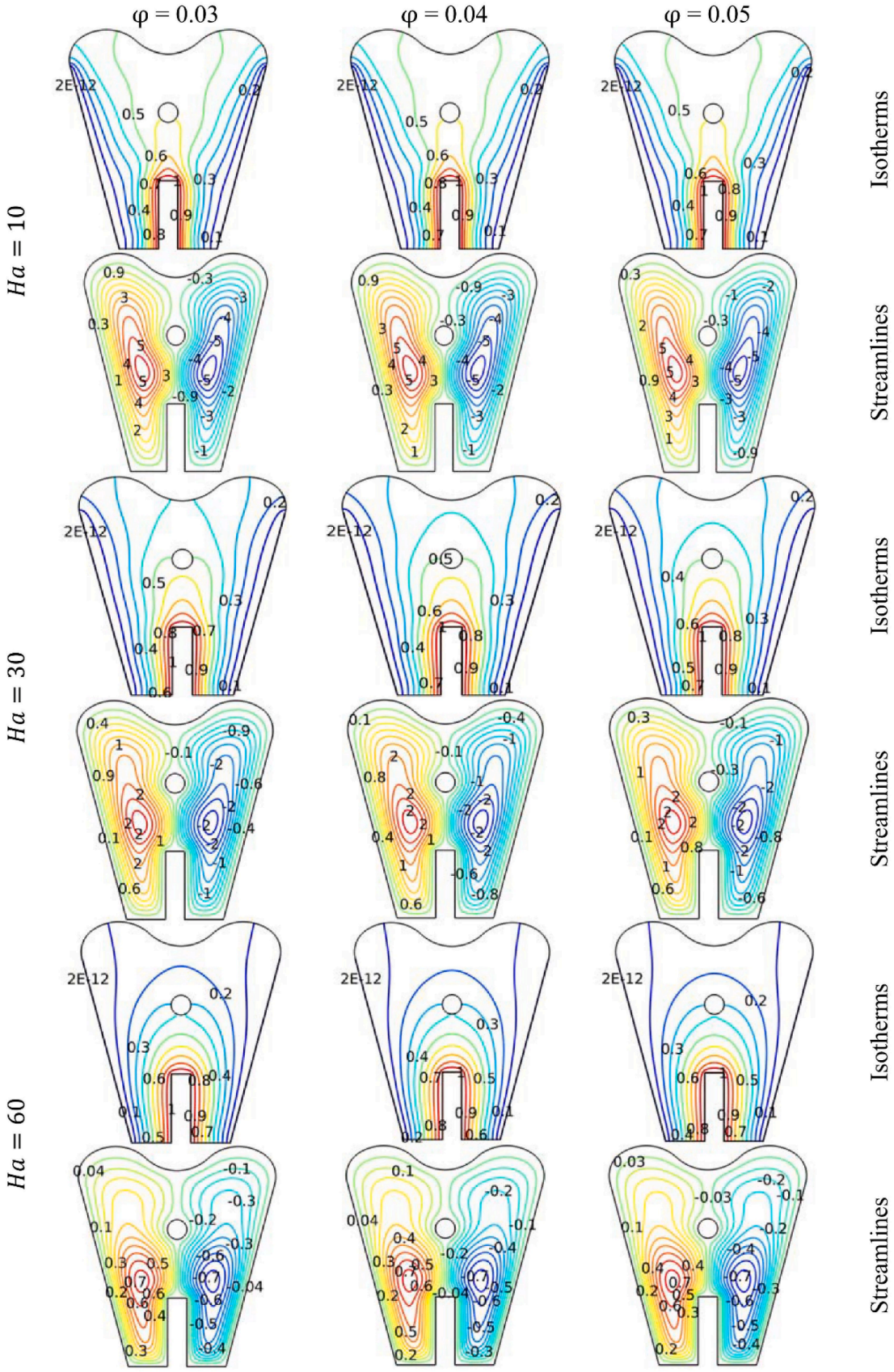


**Fig. 8.** Isotherm and streamlines contours for various φ across different Ha with Ra = $10^5$, *Pr* = 6.8377.

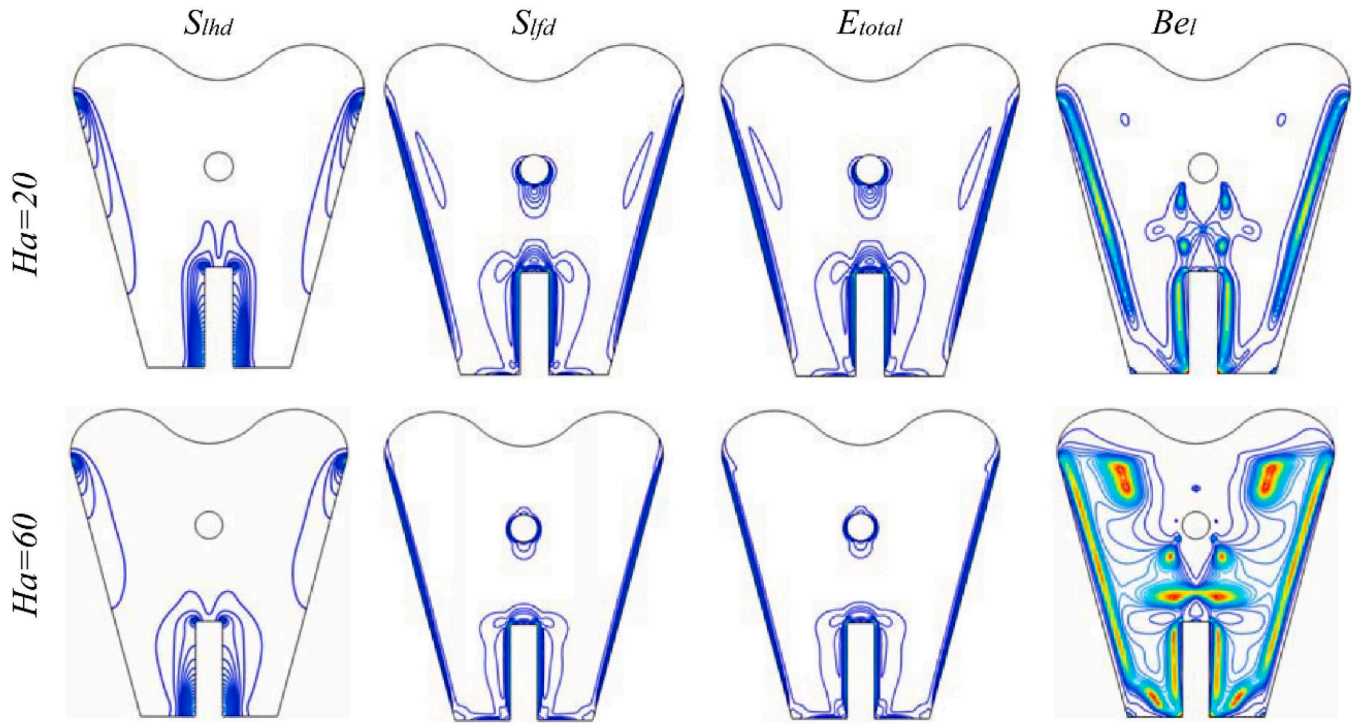


**Fig. 9.** Egen factors, including $S_{lhd}$, $S_{lfd}$, $E_{total,}$ and $Be_l$ for (i) $Ha$ = 20, (ii) $Ha$ = 60 at $Ra$=$10^6$ and φ = 0.04.

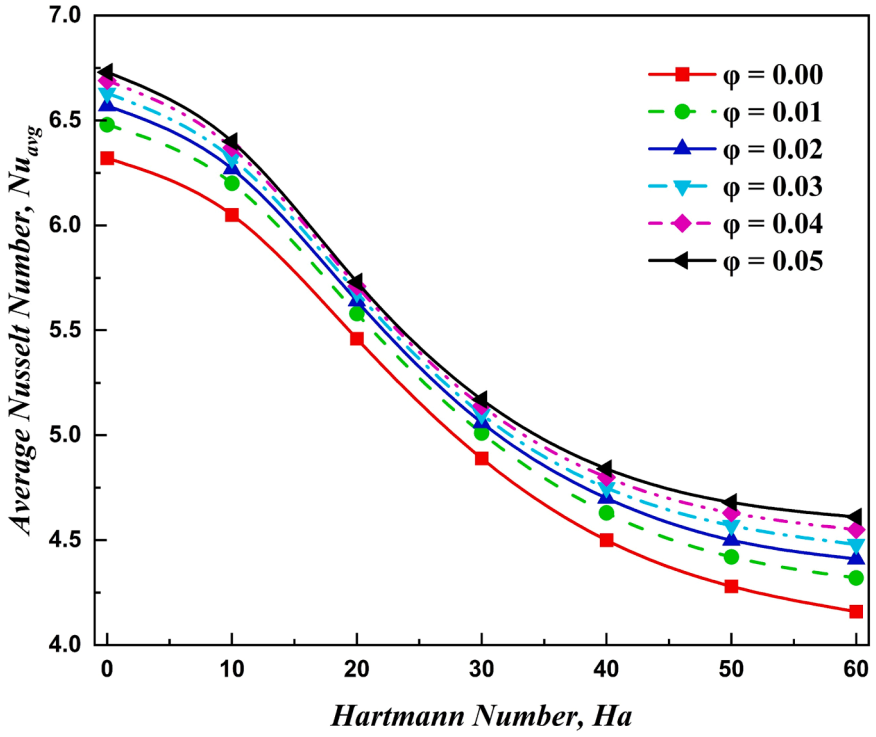


**Fig. 10.** Average Nu variation with Ha and φ for Ra = $10^5$.

- Bejan number become lowest in case-I for Ra = $10^6$ and φ = 0.00 and it increases 5.57 % by increasing volume fraction φ = (0.00 to 0.05), with fixed Ra = $10^6$ and Ha = 10.
- Be become lowest when Ha = 0 and φ = 0.00 and with increasing every φ and Ha, the corresponding Be increased and become highest at φ = 0.05, Ha = 60.

Overall, this study introduces a unique tooth-shaped cavity with wavy top walls, filled with $Al_2O_3$-$H_2O$ nanofluid and influenced by magnetic forces to boost heat transfer and control entropy generation. Nanoparticles improve heat transfer by up to 7 % under specific conditions, while the unique cavity design—featuring wavy top walls and a heated rectangular vertical wall (RVW)—optimizes space utilization and enhances heat conduction. Altogether, these features promote efficient

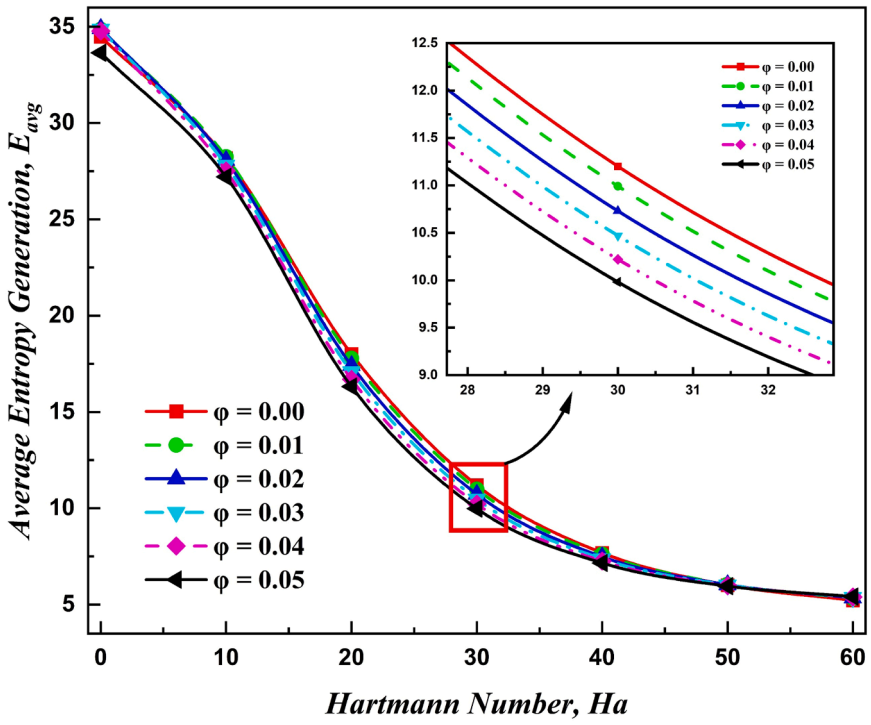


**Fig. 11.** Average Egen variation with Ha and φ for Ra = $10^5$.

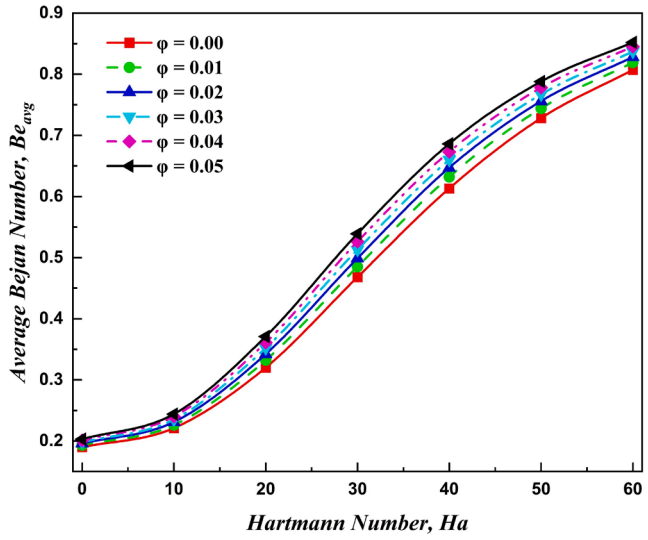


**Fig. 12.** Average Be variation with Ha and φ for Ra = $10^5$.

heat removal, supporting better performance and durability in electronic devices through optimized thermal management.

## Limitations

This study has a few limitations, as it assumes steady-state, laminar flow, which doesn't fully capture the changing and sometimes turbulent conditions seen in real-world applications. Moreover, the focus is on a specific nanofluid, $Al_2O_3$-$H_2O$, so the findings might not directly apply to other nanofluids with different properties. While the results are validated against existing studies, more hands-on experimental testing could make the conclusions even stronger.

## AI declaration

The authors used AI-assisted technology (ChatGPT 3.5) for language editing and grammar checking.

## CRediT authorship contribution statement

**Bijan Krishna Saha:** Writing – review & editing, Writing – original draft, Visualization, Validation, Supervision, Software, Resources, Project administration, Methodology, Investigation, Funding acquisition, Formal analysis, Conceptualization. **Jahidul Islam Jihan:** Writing – review & editing, Writing – original draft, Visualization, Validation, Software, Methodology, Investigation. **Goutam Barai:** Writing – review & editing, Writing – original draft, Visualization, Validation, Software, Investigation. **Nur Jahangir Moon:** Writing – review & editing, Writing – original draft, Visualization, Validation, Software, Investigation. **Goutam Saha:** Writing – review & editing, Writing – original draft. **Suvash C. Saha:** Writing – review & editing, Writing – original draft.

## Declaration of competing interest

The authors declare that they have no known competing financial interests or personal relationships that could have appeared to influence the work reported in this paper.

## Funding

The author (Bijan Krishna Saha) would like to express his sincere appreciation to the University Grants Commission (UGC) of Bangladesh with Grant No. BU/Reg/Aca/Research/2023–2024/633(Part 1)/03 for providing him financial support for conducting this research.

## Data availability

No data was used for the research described in the article.

## References


[1] G. Saha, A.A.Y. Al-Waaly, M.C. Paul, S.C. Saha, Heat transfer in cavities: configurative systematic review, Energies (Basel) 16 (5) (2023) 2338, https://doi.org/10.3390/en16052338.

[2] G. Saha, J.H. Saboj, P. Nag, S.C. Saha, Synergistic heat transfer in enclosures: a hybrid nanofluids review, J. Nanofluids 13 (2) (2024) 524–535, https://doi.org/10.1166/jon.2024.2143.

[3] G. Saha, A.A.Y. Al-Waaly, M.M. Ikram, R. Bihani, S.C. Saha, Unveiling the dynamics of entropy generation in enclosures: a systematic review, Int.J. Thermofluids 21 (2024) 100568, https://doi.org/10.1016/j.ijft.2024.100568.

[4] J.H. Saboj, P. Nag, G. Saha, S.C. Saha, Heat transfer assessment incorporated with entropy generation within a curved corner structure enclosing a cold domain, Heat Transfer (Hoboken, N.J. Print) 53 (5) (2024) 2460–2479, https://doi.org/10.1002/htj.23044.

[5] J.I. Jihan, B.K. Saha, P. Nag, N.J. Moon, G. Saha, S.C. Saha, Advancing thermal efficiency and entropy management inside decagonal enclosure with and without hot cylindrical insertions, Int. J. Thermofluids (2024) 100785, https://doi.org/10.1016/j.ijft.2024.100785.

[6] M.M. Ikram, G. Saha, S.C. Saha, Second law analysis of a transient hexagonal cavity with a rotating modulator, Int. J. Heat Mass Transf. 221 (2024) 125039, https://doi.org/10.1016/j.ijheatmasstransfer.2023.125039.

[7] T. Saha, G. Saha, N. Parveen, T. Islam, Unsteady magneto-hydrodynamic behavior of TiO2-kerosene nanofluid flow in wavy octagonal cavity, Int. J. Thermofluids 21 (2024) 100530, https://doi.org/10.1016/j.ijft.2023.100530.

[8] J.H. Saboj, P. Nag, G. Saha, S.C. Saha, Entropy production analysis in an octagonal cavity with an inner cold cylinder: a thermodynamic aspect, Energies (Basel) 16 (14) (2023) 5487, https://doi.org/10.3390/en16145487.

[9] B.K. Saha, J.I. Jihan, Md.Z. Ahammad, G. Saha, S.C. Saha, Enhanced thermal performance and entropy generation analysis in a novel cavity design with circular cylinder, Heat Transfer (Hoboken, N.J. Print) 53 (3) (2024) 1446–1473, https://doi.org/10.1002/htj.22999.

[10] M. Sheremet, I. Pop, H.F. Öztop, N. Abu-Hamdeh, Natural convection of nanofluid inside a wavy cavity with a non-uniform heating: entropy generation analysis, Int. J. Num. Methods Heat Fluid Flow 27 (4) (2017) 958–980, https://doi.org/10.1108/HFF-02-2016-0063.

[11] N. Acharya, On the hydrothermal behavior and entropy analysis of buoyancy driven magnetohydrodynamic hybrid nanofluid flow within an octagonal enclosure fitted with fins: application to thermal energy storage, J. Energy Storage 53 (2022) 105198, https://doi.org/10.1016/j.est.2022.105198.

[12] M. Mobedi, Conjugate natural convection in a square cavity with finite thickness horizontal walls, Int. Comm. Heat Mass Transfer 35 (4) (2008) 503–513, https://doi.org/10.1016/j.icheatmasstransfer.2007.09.004.

[13] M. Hatami, Numerical study of nanofluids natural convection in a rectangular cavity including heated fins, J. Mol. Liq. 233 (2017) 1–8, https://doi.org/10.1016/j.molliq.2017.02.112.

[14] Shafee, A., Haq, R.U., Sheikholeslami, M., Ali Herki, J.A., & Nguyen, T.K. (2019). An entropy generation analysis for MHD water based Fe3O4 ferrofluid through a porous semi annulus cavity via CVFEM. *Int. Comm. Heat Mass Transfer*, 108, 104295. https://doi.org/10.1016/j.icheatmasstransfer.2019.104295.

[15] A.I. Alsabery, M.A. Sheremet, M. Ghalambaz, A.J. Chamkha, I. Hashim, Fluid-structure interaction in natural convection heat transfer in an oblique cavity with a flexible oscillating fin and partial heating, Appl. Therm. Eng. 145 (2018) 80–97, https://doi.org/10.1016/j.applthermaleng.2018.09.039.

[16] M.A. Ismael, H.F. Jasim, Role of the fluid-structure interaction in mixed convection in a vented cavity, Int. J. Mech. Sci. 135 (2018) 190–202, https://doi.org/10.1016/j.ijmecsci.2017.11.001.

[17] M. Sheikholeslami, M. Gorji-Bandpy, D.D. Ganji, S. Soleimani, Natural convection heat transfer in a cavity with sinusoidal wall filled with CuO–water nanofluid in presence of magnetic field, J. Taiwan Inst. Chem. Eng. 45 (1) (2014) 40–49, https://doi.org/10.1016/j.jtice.2013.04.019.

[18] A.S. Dogonchi, M.S. Sadeghi, M. Ghodrat, A.J. Chamkha, Y. Elmasry, R. Alsulami, Natural convection and entropy generation of a nanoliquid in a crown wavy cavity: effect of thermo-physical parameters and cavity shape, Case Stud. Thermal Eng. 27 (2021) 101208.

[19] P. Sreedevi, P. Sudarsana Reddy, Effect of magnetic field and thermal radiation on natural convection in a square cavity filled with TiO2 nanoparticles using Tiwari-Das nanofluid model, Alexandria Eng. Jl 61 (2) (2022) 1529–1541, https://doi.org/10.1016/j.aej.2021.06.055.

[20] T. Tayebi, A.J. Chamkha, Entropy generation analysis due to MHD natural convection flow in a cavity occupied with hybrid nanofluid and equipped with a conducting hollow cylinder, J. Therm. Anal. Calorim 139 (3) (2020) 2165–2179, https://doi.org/10.1007/s10973-019-08651-5.

[21] G. Kefayati, Lattice Boltzmann simulation of double-diffusive natural convection of viscoplastic fluids in a porous cavity, Phys. Fluids (1994) (1) (2019) 31, https://doi.org/10.1063/1.5074089.

[22] B. Ghasemi, S.M. Aminossadati, Natural convection heat transfer in an inclined enclosure filled with a water-Cuo nanofluid, Num. Heat Transfer. Part A, Applic. 55 (8) (2009) 807–823, https://doi.org/10.1080/10407780902864623.

[23] Z. Tian, A. Shahsavar, A.A.A.A. Al-Rashed, S. Rostami, Numerical simulation of nanofluid convective heat transfer in an oblique cavity with conductive edges equipped with a constant temperature heat source: entropy production analysis, Comp. Math. Applic. (1987) 81 (1) (2021) 725–736, https://doi.org/10.1016/j.camwa.2019.12.007.

[24] T. Saha, T. Islam, S. Yeasmin, N. Parveen, Thermal influence of heated fin on MHD natural convection flow of nanofluids inside a wavy square cavity, Int. J. Thermofluids 18 (2023) 100338, https://doi.org/10.1016/j.ijft.2023.100338.

[25] Z. Mehrez, A. El Cafsi, A. Belghith, P. Le Quéré, MHD effects on heat transfer and entropy generation of nanofluid flow in an open cavity, J. Magn. Magn. Mater. 374 (2015) 214–224, https://doi.org/10.1016/j.jmmm.2014.08.010.

[26] M. Corcione, Empirical correlating equations for predicting the effective thermal conductivity and dynamic viscosity of nanofluids, Energy Convers. Manag. 52 (1) (2011) 789–793, https://doi.org/10.1016/j.enconman.2010.06.072.

[27] D. Zheng, J. Du, W. Wang, J.J. Klemeš, J. Wang, B. Sundén, Analysis of thermal efficiency of a corrugated double-tube heat exchanger with nanofluids, Energy (Oxford) 256 (2022) 124522, https://doi.org/10.1016/j.energy.2022.124522.

[28] Ashorynejad, H.R., & Shahriari, A. (2018). MHD natural convection of hybrid nanofluid in an open wavy cavity. *Results Phys.*, 9, 440–455. https://doi.org/10.1016/j.rinp.2018.02.045.

[29] C.T. Nguyen, G. Roy, C. Gauthier, N. Galanis, Heat transfer enhancement using Al2O3-water nanofluid for an electronic liquid cooling system, Appl. Therm. Eng 27 (8–9) (2007) 1501–1506, https://doi.org/10.1016/j.applthermaleng.2006.09.028.

[30] F. Mebarek-Oudina, R. Fares, A. Aissa, R.W. Lewis, N. H.Abu-Hamdeh, Entropy and convection effect on magnetized hybrid nano-liquid flow inside a trapezoidal cavity with zigzagged wall, Int. Commun. Heat Mass Transf. 125 (2021) 105279, https://doi.org/10.1016/j.icheatmasstransfer.2021.105279.

[31] E. Taskesen, M. Tekir, E. Gedik, K. Arslan, Numerical investigation of laminar forced convection and entropy generation of Fe3O4/water nanofluids in different cross-sectioned channel geometries, J. Ther. Eng. 7 (7) (2021) 1752–1767, https://doi.org/10.18186/thermal.1025984.

[32] F. Corvaro, M. Paroncini, A numerical and experimental analysis on the natural convective heat transfer of a small heating strip located on the floor of a square cavity, Appl. Therm. Eng. 28 (1) (2008) 25–35, https://doi.org/10.1016/j.applthermaleng.2007.03.018.